

Significant foreground unrelated non-acoustic anisotropy on the one degree scale in WMAP 5-year observations

Bi-Zhu Jiang^{1,2}, Richard Lieu², Shuang-Nan Zhang^{1,2,3}, and Bart Wakker⁴

ABSTRACT

The spectral variation of the cosmic microwave background (CMB) as observed by WMAP was tested using foreground reduced WMAP5 data, by producing subtraction maps at the 1° angular resolution between the two cosmological bands of V and W, for masked sky areas that avoid the Galactic disk. The resulting $V - W$ map revealed a non-acoustic signal over and above the WMAP5 pixel noise, with two main properties. Firstly, it possesses quadrupole power at the $\approx 1 \mu K$ level which may be attributed to foreground residuals. Second, it fluctuates also at all values of $\ell > 2$, especially on the 1° scale ($200 \lesssim \ell \lesssim 300$). The behavior is *random and symmetrical* about zero temperature with a r.m.s. amplitude of $\approx 7 \mu K$, or 10 % of the maximum CMB anisotropy, which would require a ‘cosmic conspiracy’ among the foreground components if it is a consequence of their existences. Both anomalies must be properly diagnosed and corrected if ‘precision cosmology’ is the claim. The second anomaly is, however, more interesting because it opens the question on whether the CMB anisotropy genuinely represents primordial density seeds.

1. Introduction

Studies of the cosmic microwave background (CMB, Penzias and Wilson (1965)), the afterglow radiation of the Big Bang, are currently in a period of renaissance after the breakthrough discovery of anisotropy by the COBE mission (Smoot et al (1992)). Confirmed with much improved resolution and statistics by WMAP (Hinshaw et al (2009)), the phenomenon

¹Physics Department and Center for Astrophysics, Tsinghua University, Beijing 100084, China.

²Department of Physics, University of Alabama, Huntsville, AL 35899.

³Key Laboratory of Particle Astrophysics, Institute of High Energy Physics, Chinese Academy of Sciences, Beijing, China

⁴Department of Astronomy, University of Wisconsin, 475 N. Charter St, Madison, WI 53706, USA

provides vital information on the primordial ‘seeds’ of structure formation. The anisotropy is attributed to frequency shift of CMB light induced by these ‘seed’ density perturbations, which has the unique property that it leads to changes in the temperature of the black body spectrum and not the shape of it. The CMB has maximum anisotropy power at the 1° scale, or harmonic number $\ell \approx 220$, with lower amplitude secondary and tertiary peaks at higher ℓ .

The Λ CDM cosmological model (Spergel et al(2007)) explains the entire power spectrum remarkably using six parameters, by attributing the peaks to acoustic oscillations of baryon and dark matter fluids, as long wavelength modes of density contrast enter the horizon and undergo causal physical evolution. CMB light emitted from within an overdense region of the oscillation are redshifted by a constant fractional amount, resulting in a cold spot, which is a lowering by δT of the black body temperature T , and is frequency independent, i.e. $\delta T/T = \delta\nu/\nu = \text{constant}$. The opposite effect of blueshift applies to underdense regions, leading to hot spots. Therefore, if the anisotropy is genuinely due to acoustic oscillations, the inferred change in T at a given region should be the same for all the ‘clean’ frequency passbands of the WMAP mission. Since a corresponding variation of the CMB flux $B(\nu, T)$ at any given frequency ν is $\delta B = (\partial B/\partial T)\delta T$ if the cause is solely δT with no accompanying distortion of the functional form of B itself, the expected δB at constant δT is then the ‘dipole spectrum’ $\partial B/\partial T$ which is well measured by COBE-FIRAS (Mather et al(1994)). Moreover, the WMAP data are calibrated w.r.t. this dipole response.

A noteworthy point about the acoustic peaks is that one needs to employ the technique of cross correlation to reduce the noise contamination at high ℓ , especially the harmonics of the second and higher acoustic peaks. Specifically one computes the all-sky cross power spectrum

$$C_\ell^{ij} = \frac{1}{2\ell + 1} \sum_m a_{\ell m}^i a_{\ell m}^{j*}, \quad (1)$$

where the indices i and j denote independent data streams with uncorrelated noise that arise from a pair of maps at different frequency bands (or same band but taken at different times), and $a_{\ell m}^i = \delta T_{\ell m}^i$ is the apparent CMB temperature anisotropy for the spherical harmonics (ℓ, m) as recorded by observation i . Since the use of multiple passbands is crucial to the accurate profiling of the acoustic oscillations, it is important that we do compare them with care, down to the level of measurement uncertainties. Only *a priori* statistically consistent maps should be cross correlated, in the sense that any real discrepancies between such maps may carry vital information about new physical processes that their cross power spectrum does not reveal. In one previous attempt to address this point (see Figure 9 of Bennett et al(2003a)) WMAP1 data downgraded to an angular resolution commensurate with COBE were used to produce a difference (subtraction) map between the two missions. When displayed

side by side with the map of the expected noise for each resulting pixel, the two maps did appear consistent. Nevertheless, this powerful method of probing the CMB anisotropy does, in the context of the specific datasets used by Bennett et al(2003a), suffer from one setback: it is limited by the sensitivity and resolution of COBE.

In another test of a similar kind, we observe that each amplitude $a_{\ell m}^i$ can further be factorized as $a_{\ell m}^i = a_{\ell m} b_{\ell}^i$, where the array b_{ℓ}^i accounts for the smoothing effects of both the beam and the finite sky map pixel size, and $a_{\ell m} = \delta T_{\ell m}$ is the true amplitude of the CMB anisotropy. The results (see Figure 13 of Hinshaw et al (2007)) indicate agreement of the variance C_{ℓ}^{ij} , hence δT_{ℓ} , within the margin of a few percent for $\ell \lesssim 400$ among the many cross power spectra formed by the various possible combinations of pairs of all-sky maps. This offers more ground for optimism, but to be definitive the remaining discrepancy needs to be demonstrably attributed to noise, instrumental systematics, or foreground emission.

The purpose of our investigation is to perform further, more revealing comparisons than the two past ones described above, initially by focussing upon the angular scale of the first acoustic peak, which is $\sim 1^\circ$. Our analysis will be done in both real (angular) and harmonic domains, because while most of the effort have hitherto been pursued in the latter, the former is the domain in which the raw data were acquired and organized.

2. The all sky difference map between the WMAP5 V and W bands

We adopted the Healpix¹ pixelization scheme to ensure that all pixels across the sky have the same area (or solid angle). Firstly the W band data is smoothed to the V band resolution. Then the whole sky map is downgraded to $\approx 1^\circ$ diameter (corresponding to `nside` of 64 in the parametrization of the WMAP database), which is not only commensurate with the scale of global maximum δT power, but also large enough to prevent data over-sampling due to the use of too high a resolution, as the size is comfortably bigger than the beam width of the WMAP V band (61 GHz) larger than that of the W band.

The resulting δT values for the two cosmological passbands of V and W, span $\approx 35,000$ clean (i.e. `ext`-masked² and foreground subtracted³) pixels, from which a $V - W$ difference map at this $\approx 1^\circ$ resolution was made. After removing the monopole and dipole residuals

¹See <http://healpix.jpl.nasa.gov>.

²`ext` is short for external temperature analysis.

³For foreground subtracted WMAP5 maps see http://lambda.gsfc.nasa.gov/product/map/current/m_products.cfm.

(the latter aligned with the original COBE dipole), this map is displayed in Figure 1 along with the corresponding pixel noise map for reference; the latter represents the expected appearance of the $V - W$ map if the CMB anisotropy is genuinely acoustic in nature, so that the map would consist only of null pixels should the WMAP5 instruments that acquired them be completely noise free. When comparing the real data map of Figure 1a with the simulated map of Figure 1b, the former appears visibly noisier on the resolution scale $\approx 1^\circ$; moreover, the Leo and Aquarius (i.e. the first and third) sky quadrants contain more cold pixels than the other half of the sky, indicative of the existence of a quadrupole residual.

The extra signals revealed by the $V - W$ subtraction map are elucidated further in respect of their aforementioned properties by examining the statistical distribution of the pixel values across the four sky quadrants. As shown in Figure 2, the distribution of the 1° anisotropy is considerably wider than that expected from the WMAP5 pixel noise for all the quadrants, by $\approx 10 \mu K$, which is $\sim 10 \%$ of the $\approx 75 \mu K$ power in the first acoustic peak, and is therefore very significant. A detailed confirmation by Gaussian curve fitting is given in Table 1.

The $V - W$ quadrupole is more subtle, and is evident in the residual plots at the bottom of each graph in Figure 2, from which a slight skewness of the data to the right is apparent in quadrants 1 and 3 (the quadrants of the CMB dipole), with 2 and 4 exhibiting the opposite behavior. For this reason, the effect does not manifest itself as shifts in the Gaussian mean value μ of Table 1. Rather, the high statistical significance of both the quadrupole and the degree-scale signals, with the former having a magnitude of $\approx 1 \mu K$, are established by computing the cross power spectra of the temperature difference maps, Figure 4. This was performed at the resolution of `nside= 64` using the `PolSpice` software⁴. From Figure 4 also, the presence of excess non-acoustic anisotropy at all harmonics $\ell > 2$, including the cosmologically important $\theta \approx 1^\circ$ angular scale, appears robust. At the 1° scale ($200 \lesssim \ell \lesssim 300$), the r.m.s. is about $7 \mu K$, or 10% of the maximum CMB anisotropy. Lastly, the $V - W$ quadrupole may be displayed in isolation by arranging the data of the subtracted map as a multipole expansion

$$\delta T(\theta, \phi) = \sum_{\ell, m} a_{\ell m} Y_{\ell m}(\theta, \phi), \quad (2)$$

and evaluating at $\ell = 2$ the amplitude

$$\delta T_\ell(\theta, \phi) = \sum_m a_{\ell m} Y_{\ell m}(\theta, \phi), \quad (3)$$

⁴Available from <http://www.planck.fr/article141.html>.

(note $\delta T_\ell(\theta, \phi)$ is always a real number if the original data $\delta T(\theta, \phi)$ are real). The ensuing whole sky map is in Figure 3, and the coordinates of the axes are in Table 2.

3. Interpretation of results

The WMAP5 $V - W$ map reveals two principal anomalies to be explained: (a) the quadrupole at $\ell = 2$, with an amplitude of $\approx 1\mu K$, and (b) the higher harmonic signals, especially the $\approx 8\mu K$ anisotropy at $\ell \gtrsim 200$ (Figure 4). Similar findings are also made by others, like the noticeable hemispherical power asymmetry in the WMAP1 analysis of Eriksen et al (2004) and confirmed in the WMAP5 data by Hoftuft et al (2009), or the large scale distribution investigated by Diego et al (2009). Also because both (a) and (b) are not small effects, claims to precision cosmology are overstatements until they are properly accounted for and the cosmological model accordingly adjusted.

Concerning (a), unlike the dipole, there is no previous known CMB quadrupole of sufficient amplitude to justify its dismissal as a cross band calibration residual. In fact, our reported amplitude of $1\mu K$ is about 7 % of the $211\mu K^2$ WMAP5 anisotropy in the unsubtracted maps of the individual bands at $\ell = 2$, which is far larger than the calibration uncertainty of $\approx 0.5\%$ (Hinshaw et al (2009)) for each band.

It will probably be more rewarding to search for remaining foreground contamination not yet removed by the standard data filtering and correction procedures of the WMAP5 team (Bennett et al(2003b), Gold et al(2009)). Thermal dust emission might have a power law spectrum with an index too close to that of the Rayleigh-Jeans tail in the V and W bands for an appreciable V - W signal, although this is an interesting scenario worthy of further study (Diego et al 2009). We consider here another possibility, viz. free-free emission from High Velocity Clouds (HVCs, Wakker et al (2009) and references therein). The clouds are moving at velocities sufficiently large for any $H\alpha$ emission from them to be outside the range⁵ of the WHAM survey, the database employed to estimate the free-free contribution to the WMAP foreground. HVC parameters for the larger and brighter clouds can reach: $n_e \approx 0.2\text{ cm}^{-3}$ and column density $\approx 3 \times 10^{19}\text{ cm}^{-2}$ (Wakker et al 2008). This corresponds to an emission measure of two units, or $6 \times 10^{18}\text{ cm}^{-5}$, or $\approx 0.6\mu K$ of V-W temperature excess (Finkbeiner D.P. (2003)), on par with the $1\mu K$ of our observed quadrupole. Moreover, as can be seen from the all-sky map of N_{HI} and an estimate of the V-W excess in Figure 5 when

⁵Example of a HVC missed by WHAM is Hill et al 2009, a cloud of unit emission measure. A notable exception (counter example) would be the HVC K-complex (Haffner et al 2001), with an emission measure of 1.1 units, that happens to fall inside the velocity window of WHAM.

they are compared with Figures 3 and 4, the strength and distribution of HVCs do appear to be responsible for a non-negligible fraction of the observed anomaly on very large scales. Further work in this area is clearly necessary, and will be pursued in a future, separate paper.

We now turn to (b), the effect that occurs on the much smaller and cosmologically most significant angular scale of 1° . Calibration issues are again immediately excluded here, since the $8 \mu K$ anomalous amplitude is on par with the pixel noise of **WMAP5** for the scale in question (Table 1). Moreover, because the subtracted $V - W$ dipole and the (unsubtracted) $V - W$ quadrupole, the latter being (a), are both relatively feeble phenomena, of amplitudes ≈ 0.2 and $1 \mu K$ respectively as compared to the $7 \mu K$ amplitude of (b), the prospect of smaller scale fluctuations having been enhanced by a larger scale one can be ruled out here. CMB spectral distortion during the recombination era, or subsequently from the Sunyaev-Zeldovich (SZ) scattering, or from other foreground re-processing that were not properly compensated by the data cleaning procedure of **WMAP5**, could all be responsible for the observed anomaly. Although the first two interactions (Sunyaev and Chluba (2008), Birkinshaw and Gull (1983)) exert much smaller influences than $7 \mu K$ (bearing in mind that the degree of SZ needs to be averaged over the scale of the whole sky), the foreground could potentially play a relevant role in a similar way as it did at very low ℓ . Thus, in respect of free-free emission by HVCs alone, until a full survey at high angular resolution is performed one cannot be certain that the emission measure from these clouds is too weak to account for our (b) anomaly. However, the action of the foreground is *systematic* in that it does *not lead to random and symmetric temperature excursions* (about zero) between two frequencies of V and W. More precisely, because the sources or sinks involved have a characteristic spectrum that differs from black body in a specific way, any widening in Figure 2 of the data distribution w.r.t. the expected simulated gaussian ought to be highly asymmetric. This obviously contradicts our findings, i.e. we note from Figure 2 that the widening of the data histogram is highly symmetric. As a result, the symptoms do not point to the foreground as responsible cause.

4. Conclusion

We performed a new way of testing the black body nature of the CMB degree scale anisotropy, by comparing the all-sky distribution of temperature difference between the **WMAP5** cosmological bands of V and W, with their expected pixel noise behavior taken fully into consideration by means of simulated data. In this way a non acoustic signal is found in the **ext**-masked $V - W$ map at the $\approx 1^\circ$ resolution of **nside** = 64, with the following two properties. It has a quadrupole amplitude $\approx 1 \mu K$ (Figures 2, 3, and 4) which may in part be attributed to unsubtracted foreground emission. It also has excess anisotropy (or

fluctuation) on all scales $\ell > 2$, including and especially the scales of $200 \lesssim \ell \lesssim 300$ where most of the acoustic power resides, and about which the anomaly we reported is in the form of a symmetric random excursion about zero temperature with a r.m.s. $\approx 8 \mu K$ (Figures 2 and 4, Table 1) which is $\approx 10 \%$ of the maximum acoustic amplitude found at $\ell \approx 220$. This type of excursion frustrates attempts to explain the effect as foreground residuals, i.e. it opens the question of whether the **WMAP** anisotropy on the 1° scale is genuinely related to the seeds of structure formation.

In any case, it is clear that both anomalies have sufficiently large magnitudes to warrant their diagnoses through future, further investigations, if the status of precision cosmology is to be reinstated.

We are grateful to the referee for very valuable suggestions towards the improvement of this paper. Lyman Page, Priscilla Frisch, Gary Zank, and Barry Welsh are also acknowledged for helpful discussions. Some of the results were obtained by means of the HEALPix package (Górski et al (2005)).

V - W		$\mu(\mu\text{K})$	error (μK)	σ (μK)	error (μK)
Quadrant 1	WMAP5	-0.23	0.15	16.23	0.13
	Simulation	0.00	0.13	14.70	0.12
	Difference Δ	-0.23	0.20	6.88	0.40
Quadrant 2	WMAP5	0.24	0.12	14.47	0.10
	Simulation	-0.04	0.12	12.10	0.10
	Difference Δ	0.28	0.17	7.94	0.24
Quadrant 3	WMAP5	-0.11	0.16	16.22	0.13
	Simulation	0.03	0.15	14.70	0.12
	Difference Δ	-0.14	0.22	6.86	0.40
Quadrant 4	WMAP5	0.40	0.13	14.80	0.10
	Simulation	-0.01	0.13	12.26	0.10
	Difference Δ	0.41	0.18	8.30	0.23

Table 1: Parameters for the gaussian curves that fitted the **WMAP5** data and the pixel noise histograms (the latter are the solid lines) of Figure 2. Each parameter uncertainty is set by the $\chi^2_{\min} + 1$ criterion, which represents the usual 68 % (or unit standard deviation) confidence interval for one interesting parameter, when the error bars shown in Figure 2 are employed for fitting both the real and pixel noise data. The difference in the width σ between the two models, which gives the distribution width of the additional random signal, is given by $(\Delta\sigma)^2 = \sigma_r^2 - \sigma_s^2$. The smaller simulated gaussian widths for quadrants 2 and 4 (relative to 1 and 3) is due to the higher exposure times there (which contain the heavily scanned ecliptic poles) leading to lower pixel noise.

V-W quadrupole location (l, b)	
hot	$(-132.1^\circ, -14.4^\circ), (48.0^\circ, 14.4^\circ)$
cold	$(-81.5^\circ, 68.0^\circ), (98.5^\circ, -68.0^\circ)$

Table 2: Orientation of the quadrupole in the **WMAP5** V-W map of Figure 3.

REFERENCES

- Bennett, C.L., et al. 2003a, *ApJS*, 148, 1
- Bennett, C.L., et al. 2003b, *ApJS*, 148, 97
- Birkinshaw, M. and Gull, S.F. 1983, *Nature*, 302, 315
- Diego, J.M., Cruz, M., González-Nuevo, J., Maris, M., Ascasibar, Y., Burigana, C., preprint(arXiv:0901.4344 [astro-ph]), *MNRAS* submitted
- Eriksen, H.K., Hansen, F.K., Banday, A.J., Górski, K.M., Lilje, P.B. 2004, *ApJ*, 605, 14
- Gold, B., et al. 2009, *ApJS*, 180, 265
- Górski, K.M., Hivon, E., Banday, A.J., Wandelt, B.D., Hansen, F.K., Reinecke, M., and Bartelmann, M. 2005, *ApJ*, 622, 759-771
- Finkbeiner, D.P. 2003, *ApJS*, 146, 407
- Haffner, L.M., Reynolds, R.J., Tufte, S.L., 2001, *ApJ*, 556, L33
- Hill, A.S., Haffner, L.M., Reynolds, R.J. 2009, *ApJ*, 703, 1832
- Hinshaw, G., et al. 2007, *ApJS*, 170, 288
- Hinshaw, G., et al. 2009, *ApJS*, 180, 225
- Hoftuft, J., Eriksen, H.K., Banday, A.J., Górski, K.M., Hansen, F.K., Lijie, P.B. 2009, *ApJ*, 699, 2
- Hou, Z., Banday, A.J., Górski, K.M. 2009, *MNRAS*, 396, 3
- Mather, J.C., et al. 1994, *ApJ*, 420, 439
- Penzias, A.A. and Wilson, R.W. 1965, *ApJ*, 142, 419
- Putman, M.E., Bland-Hawthorn, J., Veilleux, S., Gibson, B.K., Freeman, K.C., Maloney, P.R. 2003, *ApJ*, 597, 948
- Spergel, D.N., et al. 2007, *ApJS*, 170, 377
- Sunyaev, R.A. and Chluba, J. 2008, *ASPC* 395, 35S
- Smoot, G., et al. 1992, *ApJ*, 396, 1

Wakker, B.P., et al. 2008, ApJ, 672, 298

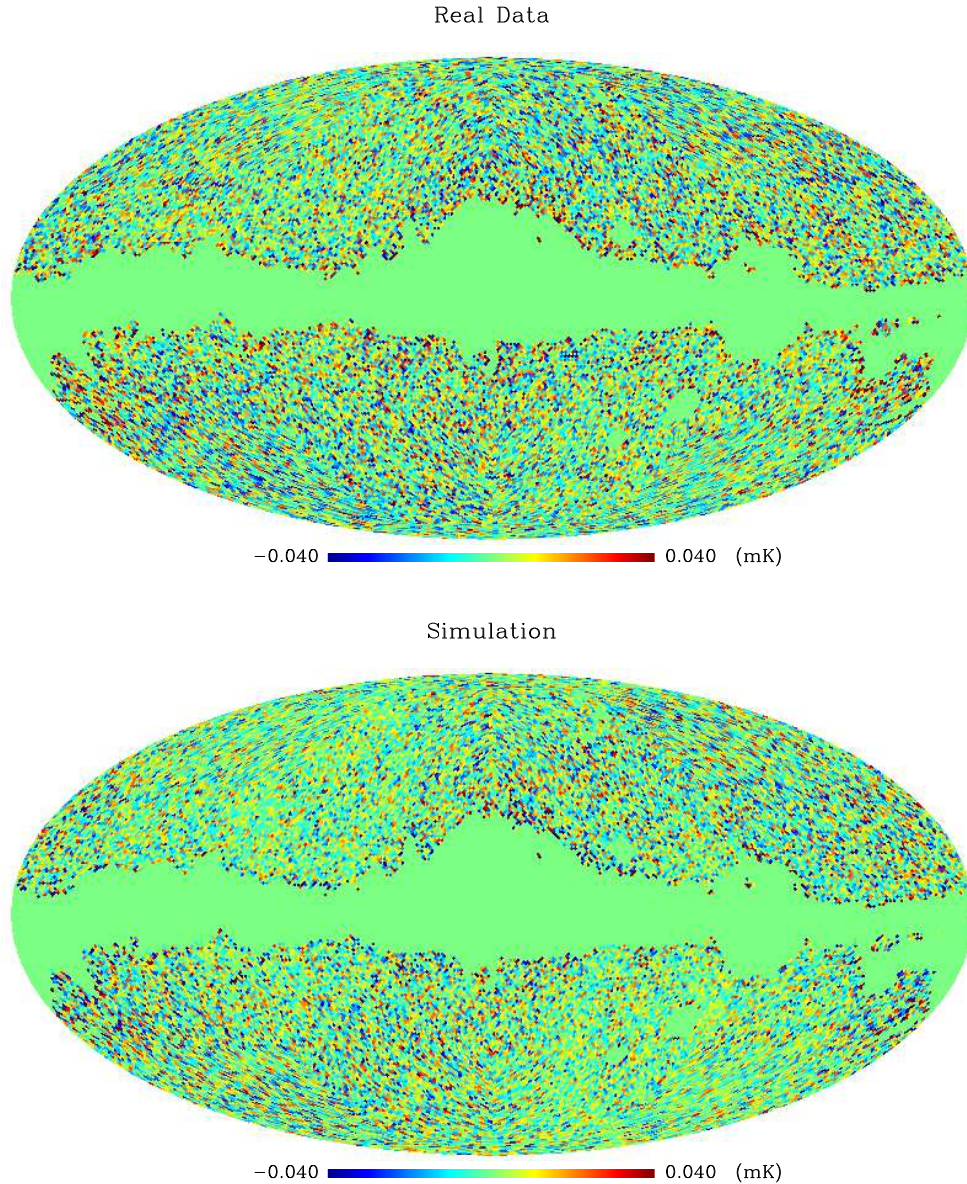


Fig. 1.— The ext-masked and point sources subtracted WMAP5 $V-W$ map, viz. the difference map between the CMB anisotropy as measured in the V band and the W band, for the real data after the removal of residual monopole and dipole components (top), and simulated pixel noise that reflect precisely the observational condition (bottom). Both maps are plotted in Galactic coordinates with the Galactic center $(l, b) = (0, 0)$ in the middle and Galactic longitude l increasing to the left. To avoid the problems of beam size variation from one band to the next, the W band data is smoothed to the V band resolution, then the pixels were downgraded to the common resolution of `nside= 64` using the foreground-reduced WMAP5 data (see section 2); this resolution under-samples the data in both bands. The color scale is coded within a symmetrical range: those pixels with values beyond $\pm 40 \mu\text{K}$ are displayed in the same (extreme) color; most of such pixels are around the masked regions. The existence of additional non- black body signal in the real data can readily be seen from this comparison, as the simulated map is noticeably quieter.

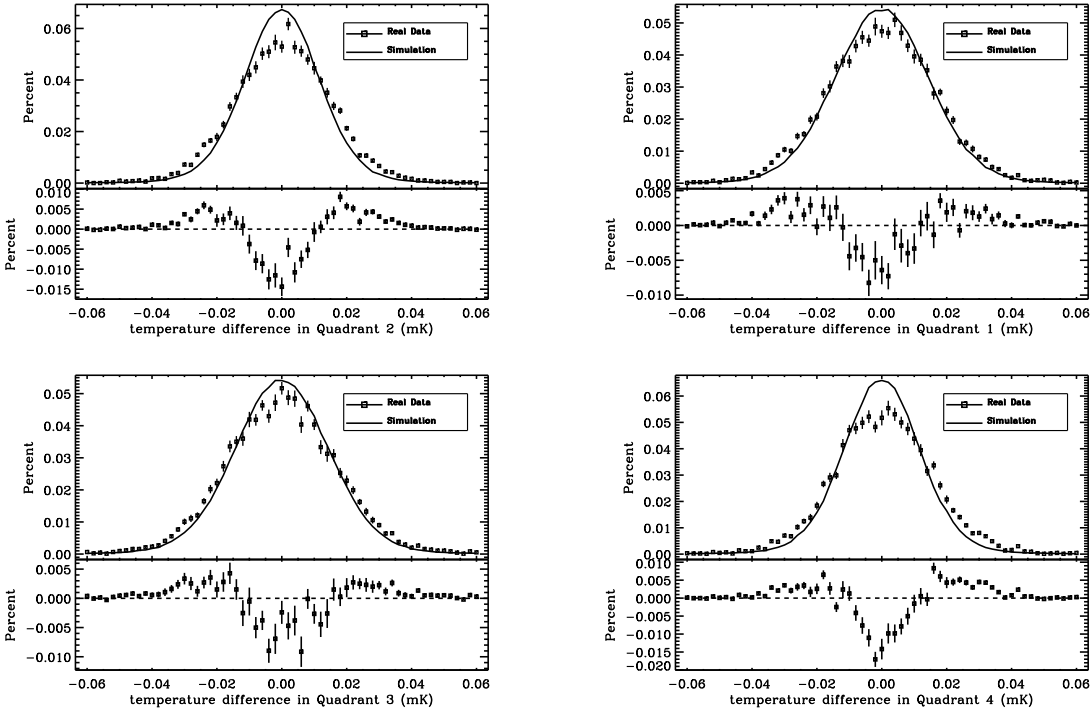


Fig. 2.— The data points show quadrant sky occurrence frequency distribution of the difference in the degree-scale ($n_{\text{side}}=64$) anisotropy between the WMAP5 V and W bands, while the errors in the data are due to the WMAP5 pixel noise for the same ext-masked quadrant sky area, i.e. they are the statistical fluctuations in the various parts of the solid line, which gives the mean histogram of this noise. The orientation of each quadrant follows the same convention as the sky maps of Figure 1, with the 1st and 3rd quadrants marking the COBE dipole.

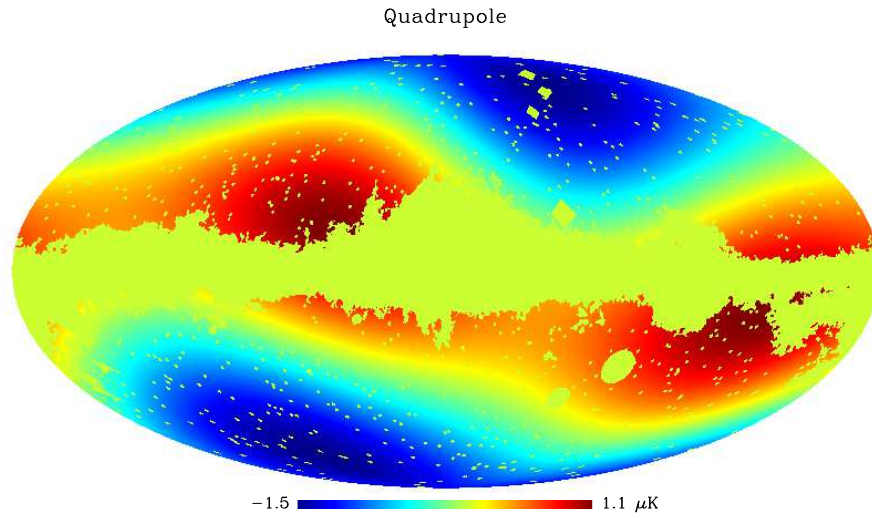


Fig. 3.— $V - W$ quadrupole of the `nside=64` WMAP5 temperature difference maps, after `ext`-masking and point source subtraction. The mathematical procedure of extracting each multipole ℓ is given in eqs. (3) and (4) of the text, and the software used to do these computations was from `anafast` of Healpix.

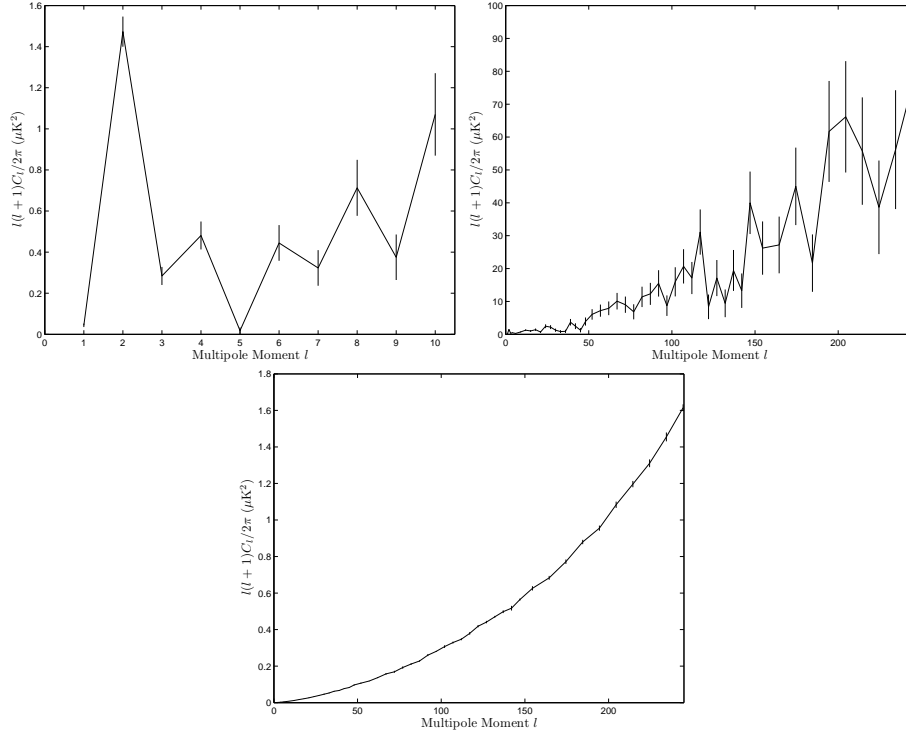


Fig. 4.— Real and simulated (noise) power spectra of the **WMAP5** $V - W$ map. These are V - W *cross* power spectra computed by cross correlating the first three years of observations with the last two. The errors in the real data of the first two graphs represent the pixel noise power of the last graph, i.e. 4c is the average of 1,000 simulated realizations of the V - W **WMAP5** pixel noise. Thus, if the noise power at harmonic ℓ is $(\delta T_\ell)^2$ from 4c, the upper error bar in 4a and 4b will extend from T_ℓ^2 to $(T_\ell + \delta T_\ell)^2$ where T_ℓ is the observed V - W anisotropy of each real data point (given by the intersection of the error bars with the zig-zag line) in 4a and 4b. The rising trend ($\sim l^2$) of all three curves towards higher l simply reflects the relatively larger pixel noise for smaller angular areas. For $l > 200$ the real data of 4a and 4b rapidly become noise dominated.

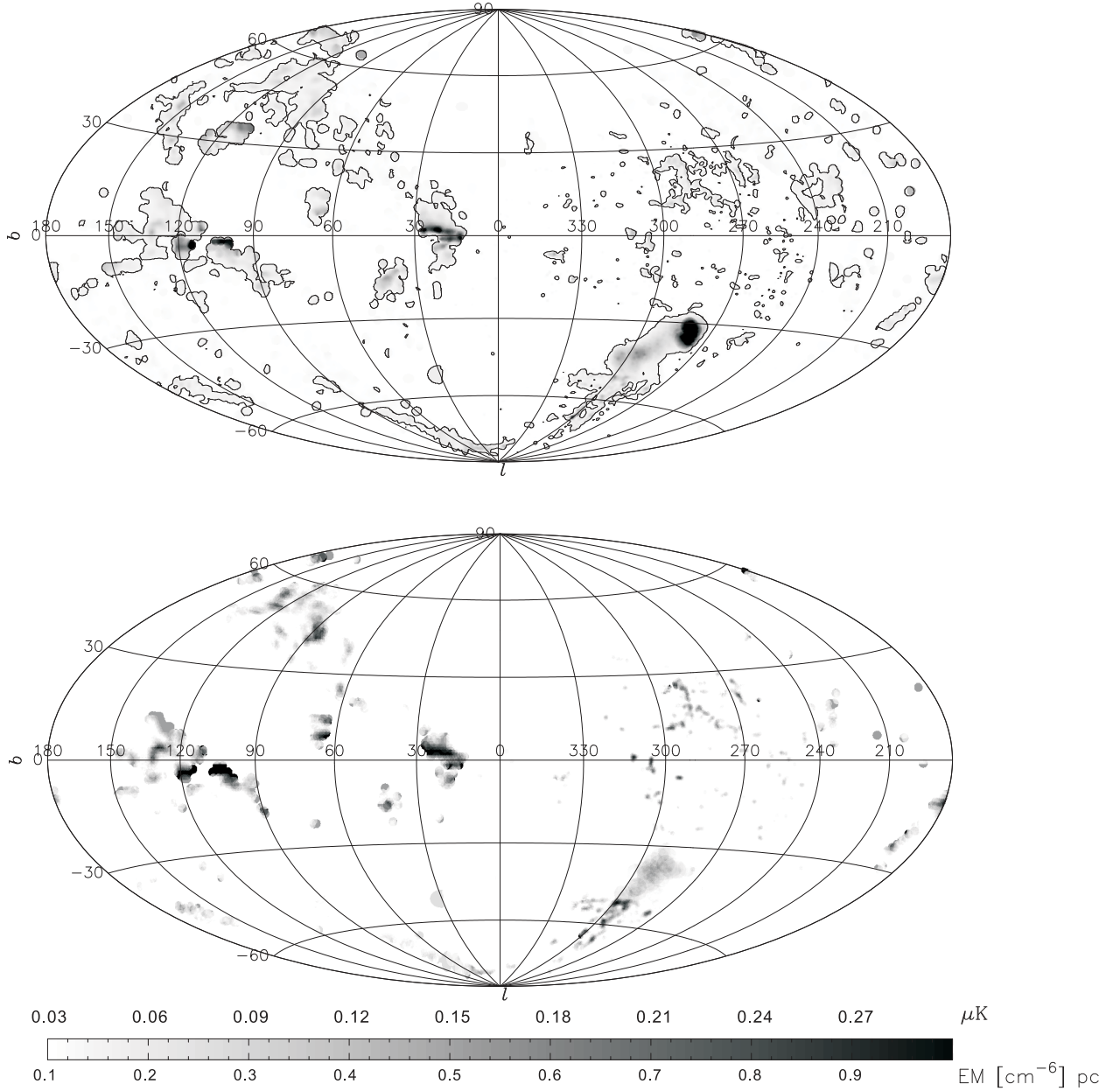


Fig. 5.— Upper map shows 21 cm data of HVCs with HI column density (N_{HI}) larger than $7 \times 10^{18} \text{ cm}^{-2}$ (i.e. the greyscale shows N_{HI} with the outer contour at $7 \times 10^{18} \text{ cm}^{-2}$). Complex C is the cloud in the region $l = 90^\circ - 130^\circ$, $b = 40^\circ - 60^\circ$. Complex A is around $l = 150^\circ$, $b = 30^\circ - 45^\circ$. The Magellanic Stream (MS) and Bridge is at $l = 280^\circ - 310^\circ$, $b < -30^\circ$. The Leading Arm of the MS, plus some other bright HVCs are at $l = 240^\circ - 300^\circ$, $b = 10^\circ - 30^\circ$. Lower map gives our estimated V-W temperature excess due to HVCs. Note that because the dynamic range of conversion from N_{HI} to this excess (via free-free emission measure EM of N_{HI}) is not linear (e.g. Putman et al 2003, Hill et al 2009). Our approach is to assign 0.5 and 1.0 unit of EM , or 0.15 and 0.3 μK of V-W excess, to every direction with $N_{\text{HI}} \geq 2 \times 10^{19} \text{ cm}^{-2}$ and $5 \times 10^{19} \text{ cm}^{-2}$ respectively.